Eur. Phys. J. B **10**, 457–464 (1999)

THE EUROPEAN PHYSICAL JOURNAL B

EDP Sciences

In plane to out of plane magnetic reorientation transition in partially ordered FePd thin films

V. Gehanno, R. Hoffmann, Y. Samson[a], A. Marty, and S. Auffret

CEA-Grenoble, Département de Recherche Fondamentale sur la Matière Condensée/Service de Physique des Matériaux et Microstructures, 17 rue des Martyrs, 38054 Grenoble Cedex 9, France

Received 13 October 1998 and Received in final form 5 February 1999

Abstract. It is demonstrated that perpendicular magnetic anisotropy may be obtained with a room temperature growth process in ordered (FePd) alloys. Indeed, using atomic layer by atomic layer epitaxy, a partial chemical ordering into the $L1_0$ structure is obtained, with a corresponding intermediate perpendicular anisotropy ($K_u/2\pi M_s^2 \sim 0.4$). These samples provide an appropriate template for the study of the magnetic reorientation from in plane to out of plane magnetization upon layer's thickness increase. VSM, transverse Kerr measurements and magnetic force microscopy have been used in order to determine the relevant magnetic parameters and the occurrence of the reorientation transition.

PACS. 75.70.-i Magnetic films and multilayers

1 Introduction

Chemically ordered alloys have been successfully used to elaborate perpendicularly magnetized thin films [1–4]. These recent results rely on the ability to induce the growth of the thin films with the easy axis of the ordered phase along the normal direction to the film plane. For instance, the FePd system exhibits a phase transition at the equiatomic composition around 920 K between a disordered face-centered-cubic phase and an $L1_0$ (CuAu-I type) ordered tetragonal structure [5]. This ordered structure consists in alternating Fe and Pd atomic planes so that it retains only one of the four fold symmetry axis existing in the disordered alloy. The ordered alloy exhibits a high magnetocrystalline anisotropy, the four fold symmetry axis being an easy magnetization axis [6,7]. It was shown that the codeposition of the alloy at a high temperature leads to a high degree of chemical order, both on a long range and a short range scale, and this results in perpendicularly magnetized thin films [8,9]. This configuration has attracted a large interest due to the potential of ordered alloys (FePt [10], FePd [9]...) for high density magnetic recording applications. As an alternative to this growth procedure, it was proposed to artificially grow the ordered phase by depositing alternate atomic layers of pure Fe and Pd. This method can be seen as an attempt to artificially obtain the $L1_0$ structure, and then a perpendicular magnetic anisotropy at room temperature. Indeed, $L1_0$ ordered samples can be seen as an ultimate multilayer with a bi-atomic period. A structural study has shown that this layer by layer growth process leads to an intermediate degree of chemical order on the short range scale but a very low degree of order on a long range scale [11]. Here we investigate the magnetic properties of these partially ordered samples. First we evaluate the magnetic anisotropy from magnetization curve measurements. Next we investigate the transition from an in-plane to an out-of-plane magnetization with transverse Kerr measurements and Magnetic Force Microscopy (MFM) observations. This transition is allowed by the evolution of the balance between the magnetostatic energy and the energy associated with the uniaxial anisotropy when the thickness of the magnetic layer increases. A similar transition has been observed in ultrathin magnetic layers such as Ag/Fe/Ag(100) as the weight of the anisotropy induced by the interfaces decreases as thickness increases, thereby not allowing to maintain a perpendicular magnetization [12]. Finally, we confront our experimental data with the models proposed by Sukstanskii and Primak [13] which allow to forecast the direction of the magnetization depending on the thickness of the thin film and the magnetic anisotropy of the material.

2 Elaboration and structure

The samples were prepared by Molecular Beam Epitaxy under Ultra-High vacuum (10^{-7} Pa). A 2 nm seed layer of Cr was deposited onto a MgO (001)-oriented substrate in order to induce the epitaxial growth of the 60 nm single crystal Pd buffer layer. In order to smooth the Pd surface, the sample was then annealed during 10 minutes at 700 K. The deposition of the alloy layers then consisted in alternatively depositing atomic layers of pure Fe and

[a] e-mail: ysamson@cea.fr

pure Pd at room temperature, using a constant evaporation time for each layer. The Pd and Fe fluxes from the electron beam evaporators were first adjusted using the RHEED intensity oscillations corresponding to the growth of both pure Pd and FePd alloy at room temperature on a calibration sample. Thereafter, Fe and Pd fluxes were both set to 0.2 monolayer (ML) per second and the shutters of each evaporator were alternatively opened for 5 s. By masking progressively the fluxes with a motorized shutter, a 15 mm long wedge sample was grown under these conditions, with its thickness varying between 0 and 45 nm. The motorised shutter is close enough to the sample so that imperfect shadowing effects are negligible. The RHEED diagram revealed the cube-on-cube relationship (001)[001]Pd/(001)[001]FePd. The alloy layer was finally covered with a 2 nm Pd layer to prevent oxidation.

A detailed investigation of the structure of a flat sample, prepared in the same way than the one studied here, has been reported elsewhere [11]. X-ray diffraction experiments were used to evaluate the degree of long-range order S in the layer, defined as $S = |n_{\mathrm{Fe}} - n_{\mathrm{Pd}}|$ where $n_{\mathrm{Fe(Pd)}}$ stands for the site occupancy on the Fe(Pd) sublattice. This parameter S ranges from 0 for a completely disordered film to 1 for a perfectly ordered film. The result of the measurement ($S \sim 0.1$) then evidenced a low degree of long range order in the samples. In addition, the analysis of EXAFS spectra allowed to investigate the directional short range order in the samples, revealing a high anisotropy of the chemical order in the first coordination sphere. Indeed, a central Fe atom is surrounded by 87% (resp. 38%) of Fe atom when considering the neighbours in the out-of-plane direction (resp. in the plane direction).

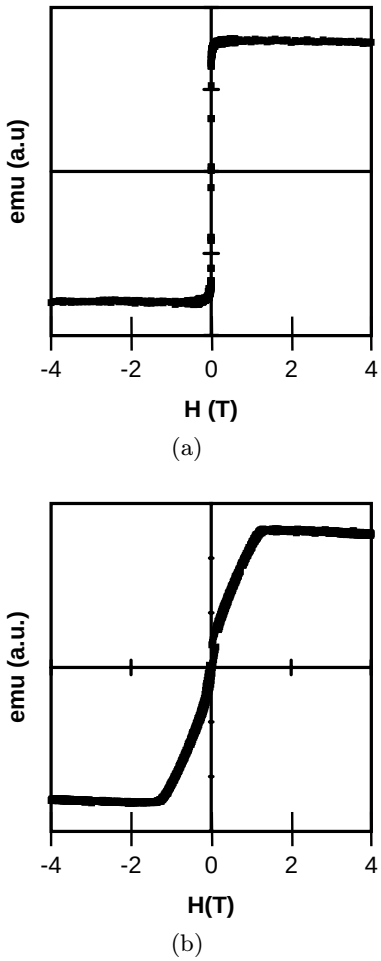

Fig. 1. Magnetization curves measured using a VSM with in-plane (a) and out-of plane (b) magnetic fields. The layer thickness of the involved part of the wedged sample varies from 18 to 27 nm. The easy axis lies into the plane of the layer. The calculation of the anisotropy constant from the area between the these curves and the similar ones obtained at other thicknesses reveals a weak perpendicular anisotropy: $K_{\mathrm{u}} = 2.6 \times 10^6$ emu/cm^3.

3 Perpendicular magnetic anisotropy

The magnetization curves (Fig. 1) were measured using a Vibrating Sample Magnetometer (VSM) with the applied field either parallel or perpendicular to the layers plane. To allow these measurements, the wedge sample was divided in five parts, each extending over a thickness range of 9 nm and measured successively in the VSM. The hysteresis curves reveal that the easy axis of the samples lies in the plane of the layers. The saturation magnetization was evaluated from extensive measurements on other FePd thin layers: $M_{\mathrm{s}} = 1030$ emu/cm^3 [9]. This value is in close agreement with the ones determined for bulk iron palladium alloys (1050-1100 emu/cm^3 [14–16]). The area between the two (in plane and perpendicular to the plane) magnetization curves gives access to the energy gained by the sample when the magnetization evolves from an in plane to an out of plane monodomain configuration. Since this energy equals the difference $K_{\mathrm{u}} - 2\pi M_{\mathrm{s}}^2$ [17], this allows to evaluate the uniaxial anisotropy constant K_{u}. We find a mean value (averaged on the five parts of the sample) $K_{\mathrm{u}} = 2.6 \times 10^6$ emu/cm^3, corresponding to a low value of the quality factor

$$\hat{K} = \frac{K_{\mathrm{u}}}{2\pi M_{\mathrm{s}}^2} = 0.4.$$

No significant variation of the uniaxial magnetic anisotropy with the thickness of the layer was found in the wedge sample. This kind of material with a weak uniaxial perpendicular anisotropy is likely to exhibit a so-called stripe structure [18] above a critical thickness h_{c}: for low thicknesses, the magnetization lies in the plane of the layer, while for thicknesses above h_{c}, an out-of plane component of the magnetization appears due to instability of the magnetization direction [13]. The magnetization points then alternatively upwards and downwards forming a stripe configuration. Such a configuration has been recently imaged in Co thin films [19]. As the thickness increases, the magnetization tends to be more and more perpendicular to the film plane, corresponding to a decrease of the in-plane component of the magnetization, while the width of the stripe structure increases.

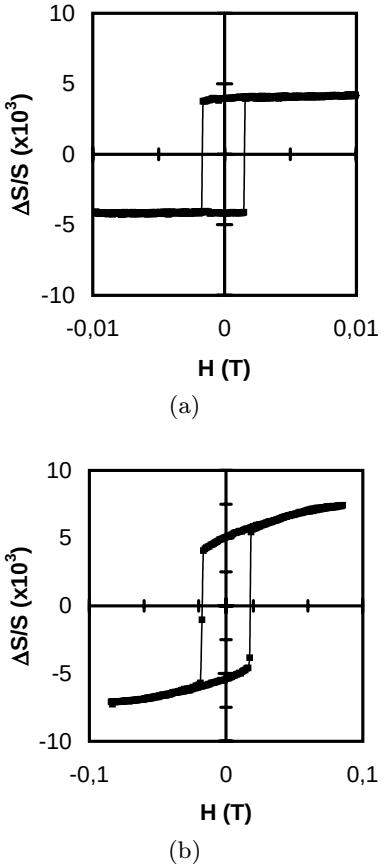

Fig. 2. Transverse Kerr effect measurements (Kerr signal as a function of the applied in plane field H). S is the amplitude of the signal corresponding to the light reflected by the sample, ΔS is its modification as a function of the applied field. The FePd layer thicknesses are: (a) $h = 16$ nm (below the critical thickness h_c), (b) $h = 35$ nm (larger than h_c). Note the large difference in the coercitive fields.

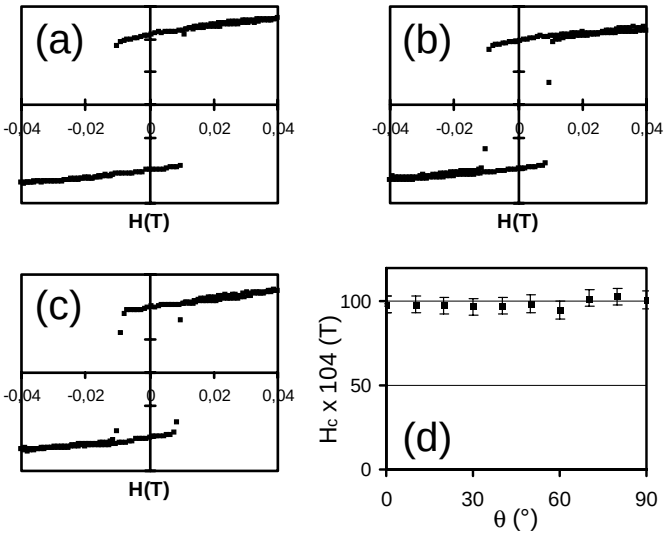

Fig. 3. Transverse Kerr effect measurements. The FePd layer thickness is $h = 32$ nm. The sample has been rotated with respect to one of the (100) in plane: (a) $\theta = 0°$, (b) $\theta = 30°$, (c) $\theta = 60°$. (d) The coercitive field is plotted as a function of the angle with respect to one of the (100) direction. There is no significant variation of this parameter. In this figure, the amplitude of the Kerr signal is not calibrated.

4 Transverse Kerr effect measurements

We have measured the in-plane magnetization curves of the sample in the low field range using a Kerr facility (Fig. 2). Here, the magnetic signal originates from the transverse Kerr effect: the external field is applied in the plane of the layer, perpendicularly to the reflexion plane of the light. The incident light is emitted by a laser diode (670 nm) with an incident angle of 60° (with respect to the sample plane). The spot size on the sample is about 1 mm in diameter, so that, due to the wedged shape of the FePd layer, the thickness range of the area over which the signal is averaged is about 3 nm. The ratio $\Delta S/S$ (S being the amplitude of the signal corresponding to the light reflected by the sample) plotted in Figure 2 is proportional to the in-plane component of the magnetization. These measurements also allows to address the issue of possible in plane easy axis within the sample. In Figure 3, three hysteresis curves are reported, corresponding to magnetic fields applied along various directions with respect to one of the (100) axis. In addition, the evolution of the coercitive field as a function of the angle with respect to one of the in plane (100) directions is displayed. These data demonstrates that neither the quantitative (coercitive field), neither the qualitative (shape of the hysteresis curves) aspects of the hysteresis curves depend on the direction of the applied field within the plane, thereby suggesting the absence of any significant in plane anisotropy. Figure 4a displays the variation of the value of the remanent signal at zero field, as a function of the thickness of the magnetic layer. The singular behaviour observed at 29 nm (compare also Figs. 2a and 2b) can be related to the occurrence of the stripe configuration as described in the above paragraph. Indeed, for thicknesses smaller than 29 nm, the magnetization is expected to lie in the plane of the layer. In this configuration, the quantity of material contributing to the signal increases proportionally to the thickness of the sample, leading to the observed increase in the remanent signal. Above the critical thickness, as the magnetization adopts an out-of plane component, the Kerr remanent signal is decreasing in spite of the thickness increase. This shows that the average in-plane component of the magnetization is decreasing, thus leading to the conclusion that the magnetization tends to be more and more perpendicular to the layer plane.

The transition from the in-plane to the out-of plane magnetization configuration also affects the coercitivity (Fig. 4b). For thickness smaller than 29 nm, the coercivity is less than 30 Oe. It decreases with increasing thickness, indicating that the pinning of the magnetic walls on the interfaces plays an important role to explain the evolution of the coercitivity. Indeed, a large number of magnetic domain walls appears above the critical thickness and these walls may be responsible for a far larger coercivity through

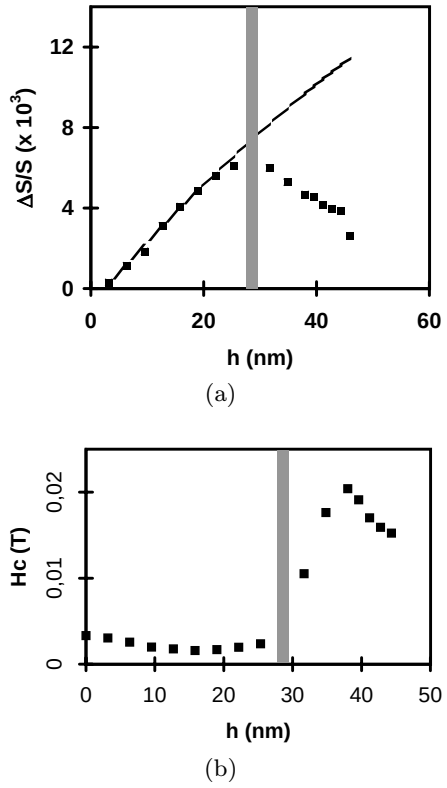

Fig. 4. These data have been extracted from transverse Kerr effect measurements. Part (a) displays the evolution of the in plane remanent signal upon layer thickness. The value of the ratio of the $\Delta S/S$ (S being the amplitude of the signal corresponding to the light reflected by the sample, ΔS being its modification as a function of the field) is plotted as a function of the layer thickness. Below the critical thickness, the remanence stays at a 100% value with respect to the saturation one (square hysteresis curve) and the Kerr signal increases almost linearly as the thickness increases. The dotted line corresponds to an extrapolation of the amplitude of the Kerr signal which would still correspond to a 100% remanence. This extrapolation is based on a polynomial fit of the experimental values obtained below the critical thickness, together with an additional VSM data giving the ratio of the remanent to saturated between $h = 27$ and $h = 36$ nm. The wide grey line outlines the critical thickness (according to the discussion in the text). Part (b) displays the evolution of the coercitive field upon layer thickness. See Figure 2 for two examples of the experimental Kerr hysteresis curves.

pinning to the interfaces or others defects. Once the new magnetic configuration has been established, the coercivity decreases again (but from a higher value) when the layer thickness increases. This behavior is in agreement with the idea that the main source of the coercivity is at the interfaces.

5 Magnetic configuration of the sample

5.1 Critical thickness - magnetic force microscopy

The analysis of the remanent signal and the coercivity obtained from the in-plane magnetization curves allowed to evaluate the critical thickness h_c. As an independent way to investigate the transition from the in-plane to the out-of plane magnetization configuration, the samples were studied by MFM. The measurements were performed using a Nanoscope IIIa from Digital Instruments, in the ac mode where the force gradient (second derivative of the magnetic field) between a magnetic tip and the sample is detected. Here, the tip was magnetized along the normal to the sample: the measurement was then sensitive to the perpendicular component of the stray field emerging from the layer. For thicknesses smaller than 27 nm, no magnetic contrast could be observed, leading to the conclusion that the magnetization lies into the plane of the layer (with in plane domain sizes far above the reasonable scan sizes). For thicknesses above 27 nm, the images (Fig. 5) reveal the existence of a periodic component of the magnetization pointing out of the plane of the layer. This configuration corresponds to the stripe structure postulated above. The experimental value of the critical thickness h_c as deduced from the MFM measurement (27 nm) is in excellent agreement with the value deduced from the in-plane magnetization curves (29 nm).

5.2 Critical thickness - model

As already pointed out, the stripe structure has been theoretically predicted by various authors. Sukstanskii and Primak have providen a parametric expression relating the critical thickness h_c to the anisotropy constant K_u [13]. The corresponding equations may be written in reduced units as below:

$$\hat{K} = \frac{K_u}{2\pi M_s^2} = \frac{1}{2\pi}\left(3v - (\pi + 3v)e^{\frac{-\pi}{v}}\right) \quad (1)$$

$$\frac{h_c}{h_s} = \frac{\sqrt{2}\pi^{3/2}}{v}\left(v - (\pi + v)e^{\frac{-\pi}{v}}\right)^{-1/2} \quad (2)$$

where $h_s = \sqrt{\frac{A}{2\pi M_s^2}}$ and A is the exchange constant. Equations (1, 2) are linked by the parameter v.

These equations have been obtained from a classical form of the magnetic energy including exchange, anisotropy and magnetostatic energy, and by using a sinus-jacobi profile for the out-of plane component of the magnetization as a trial function. The energy has been minimized with respect to the amplitude of the perpendicular magnetization and the domain size. The in-plane component of the magnetization is assumed to be parallel to the stripe direction and the magnetization vector is uniform across the layer's thickness. However, it is demonstrated in Appendix that the critical thickness does not depend on the choice of the (sinus Jacobi) magnetic profile. Indeed, equations (1, 2) are easily obtained by using a sinus profile for the magnetization angle.

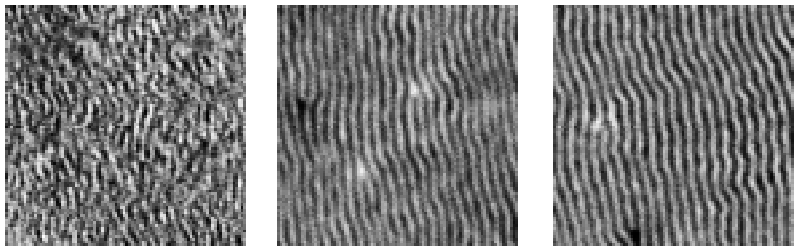

Fig. 5. 2 μm $\times$ 2 μm from Magnetic Force Microscopy images of the zero field magnetic configuration (as grown sample). A similar configuration is obtained after the application of an in-plane saturating field. The corresponding thicknesses h of the FePd layer (and measured stripe widths d) are: (a) $h = 28$ nm ($d = 37.5$ nm), (b) $h = 34$ nm ($d = 41$ nm), (c) $h = 45$ nm ($d = 48.5$ nm). In order to maintain a clear contrast between up and down stripes on the three images, the grey scale has been adjusted for each image. As a result, the images do not reproduce the decrease of the contrast as the thickness decreases.

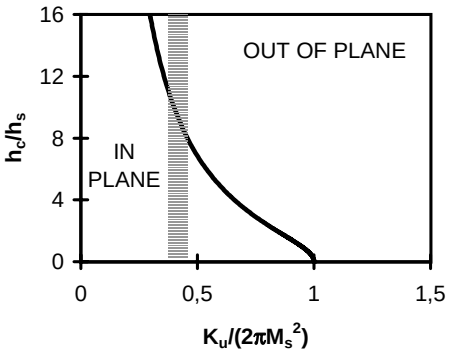

Fig. 6. This graph outlines the transition between in plane and out of plane magnetization as a function of the thickness (h) and the perpendicular anisotropy (K_u). The black line corresponds to the critical thickness h_c. Above h_c, an out of plane component of the magnetization appears by means of the so called stripe structure. The model used here assumes a classical form for the magnetic energy and a unidimensional dependence of the out of plane component of the magnetization. The wide grey line corresponds to the wedged sample studied here, with a predicted critical thickness around 32 nm. For this sample, $h_\mathrm{s} = 3.2$ nm.

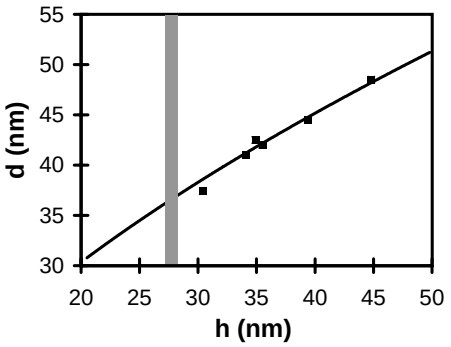

Fig. 7. Stripe width d as a function of the layer thickness h as deduced from Magnetic Force Microscopy images. The thick vertical grey line corresponds to the lowest thickness at which a stripe structure has been detected. The thin black line corresponds to the best linear fit of the domain width, using a power law dependence of the thickness of the FePd layer (both the prefactor and the exponent are free parameters).

Using equations (1, 2), the reduced critical thickness can be plotted as a function of the reduced anisotropy constant $K = K_\mathrm{u}/2\pi M_\mathrm{s}^2$. This curve splits the (h, K) space into two areas corresponding to in plane and out of plane magnetization as shown in Figure 6. The thickness (ranging from 0 to 45 nm) and the quality factor ($\hat{K}$) of the FePd wedge sample has also been reported in this figure. According to the model, the layer should exhibit a stripe structure for thicknesses above $h_\mathrm{c} = 32$ nm. This value is in a striking good agreement with the experimental results.

5.3 Stripe width - experimental data (MFM)

We now focus on the evolution of the stripe width with the thickness of the layer (Fig. 7). For thicknesses just above the critical thickness, the width of the stripes is only 37 nm and increases thereafter gradually to 48.5 nm at $h = 45$ nm. The experimental data are well fitted by a power law (the prefactor and the exponent being left free): $d = (5.44)h^{0.57}$. The corresponding curve has been reported with the experimental data in Figure 7.

5.4 Stripe width - model

The prediction obtained from the model of Sukstanskii and Primak are far less accurate on the domain width than on the critical thickness. Indeed, for a given thickness, the theoretical value is significantly lower than the experimental one: for $h = 40$ nm, the model predicts $d = 32$ nm while MFM measurements provide $d = 44.5$ nm. This discrepancy may originate from the fact that the model assumes no variation of the magnetization direction across the samples thickness. In our case, the partially ordered FePd alloy has a weak anisotropy, so that closure domains are likely to form. These domains correspond to a rotation of the magnetization towards the plane of the layer and perpendicularly to the stripe direction. This effect can be quite important close to the sample's surface. It allows a reduction of the magnetostatic energy cost of the

out-of plane component of the magnetization and hence leads to an increase of the period of the stripe configuration. However, this phenomena can be neglected near to the critical thickness as the amplitude of the z component of the magnetization is too low to favor the formation of such closure domains (which have a cost through exchange interaction).

6 The in plane to out of plane transition

6.1 From magnetic force microscopy

It is worth noting that, to our knowledge, the period of the stripe structure near the critical thickness (27 nm) is the smallest one which has been observed in a thin layer. This is due to the fact we have been able to image the domain structure near to the critical thickness (thus taking advantage of the decrease in the domain size before the out of plane to in plane transition). As a drawback, the observed lateral dimensions of the domains are quite close to the expected resolution in Magnetic Force Microscopy and it is difficult to extract quantitative information concerning the magnetization direction from the MFM images.

6.2 The in plane to out of plane transition - quantitative use of the Kerr measurements

However, a more precise knowledge of the magnetization configuration in the stripe structure may be obtained from the Kerr and VSM experiments. Indeed, it has already been pointed out that the in-plane component of the magnetization corresponds to the remanent signal in the transverse Kerr hysteresis loop (Fig. 4a). Besides, the VSM measurement provides the ratio of the in-plane component to the total magnetization, measured in the saturation state at a large field. By using the hysteresis curve obtained by the VSM on a part of the sample choosen above the critical thickness, we can extrapolate the Kerr signal corresponding to the sample saturated in the plane above the critical thickness (Fig. 4a). These data can be used to specify the profile of the magnetization. The following function has indeed been proposed to describe the magnetization angle across a stripe structure [18], and is similar to the one used by Sukstanskii and Primak [13]:

$$\sin\theta(x) = \sin(\theta_0)\mathrm{sn}\left(\frac{x}{\Delta}\middle|\sin(\theta_0)\right) \tag{3}$$

where $\Delta = \sqrt{\frac{A}{K_u}}$ and $\mathrm{sn}\,(u|k)$ is the sinus-amplitude Jacobi function [18].

θ_0 is the largest angle of the magnetization vector with respect to the plane of the sample (obtained at the center of the stripes).

The above function has been derived from the variational minimisation of a magnetic energy expression involving only anisotropy and exchange terms. It provides a parametrised function as a template for the present problem.

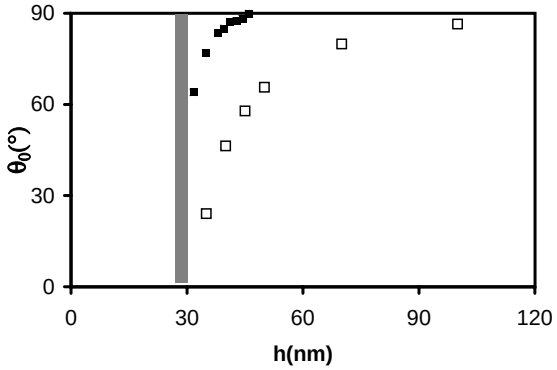

Fig. 8. (■) Maximum angle (with respect to the layer plane) of the magnetization at the middle of the stripes as a function of the layer thickness. These data have been extracted from the evolution of the in plane remanence in transverse Kerr effect measurements, by assuming a sinus-Jacobi profile for the out of plane component of the magnetization. (□) Maximum angle according to the model proposed by Sukstanskii [13]. The wide grey line corresponds to the position of the magnetic reorientation transition according to Kerr and MFM measurements.

To use equation (3) implies we neglect any component of the magnetization perpendicular to the stripe structure and across the thickness of the layer, and so the likely presence of closure domains. By comparing the projection of the magnetization vector in the plane of the sample for the sinus-amplitude Jacobi profile to the experimental Kerr data, it is possible to extract the angle θ_0. Indeed:

$$\frac{M_r}{M_s} = \frac{\int_0^{x(\theta_0)} \cos(\theta)\delta x}{\int_0^{x(\theta_0)} \delta x}\,. \tag{4}$$

Here, the Jacobi functions being the inverse of elliptic functions, we have:

$$\delta x = \Delta \frac{\delta\theta}{\sqrt{\cos(\theta)^2 - \cos(\theta_0)^2}} \tag{5}$$

where Δ is related to the wall width. The remanent magnetization and the maximum angle are then linked by the elliptic function of first kind K.

$$\frac{M_r}{M_s} = \frac{\pi}{2K(\sin(\theta_0)^2)}\,. \tag{6}$$

Some authors have considered Δ as a free parameter to obtain a more accurate description of the magnetization profile [13]. However, this does not change equation (6).

The results obtained from equation (6) are shown in Figure 8. They demonstrate that the in plane to out of plane transition occurs quite progressively, as the magnetization departs first slightly from the plane and is pointing up and down only up to intermediate angles. Thereafter, the area of nearly perpendicular magnetization widen at the middle of the stripes while the width of the domain walls diminishes. It is worth noting that the results of the model are consistent with the evolution of the contrast in Magnetic Force Microscopy images: indeed, the

contrast between up and down stripes decreases rapidly with decreasing thickness, far more rapidly than could be expected from the linear thickness decrease and from the slow diminution of the stripe period. The Suskstanskii and Primak model fails to predict correctly the maximum angle of the magnetization and hence strongly underestimates the perpendicular component of the magnetization at a given thickness (see Fig. 8). Once again, one may argue that the occurrence of closure domains allows an higher emergence angle with a lower cost in magnetostatic energy, thereby reducing the thickness range over which most part of the magnetic reorientation occurs.

7 Conclusion

FePd thin layers with perpendicular anisotropy have been prepared through a room temperature growth process, using layer by layer epitaxy. In such samples, the reproducibility of the obtained order and perpendicular anisotropy is of special concern, since a critical dependence on the precision of the calibration and on the stability of the fluxes may be expected. Indeed, it cannot be expected to deposit exactly one monolayer of each element through all the growth process. However, a large discrepancy has not been observed as different samples elaborated in the same way exhibit very similar magnetic properties. This may be seen as a clue that the perpendicular anisotropy depends essentially on the local order which is here forced by the growth process (Fe-Pd pairs along the growth direction perpendicular to the layer plane). Such an origin for the perpendicular anisotropy has been suggested in CoPd alloys [20,21].

The in plane to out of plane reorientation transition has been carefully observed. The critical thickness has been determined by using various independent approaches: domain structure observation by MFM, hysteresis curves measurements through Kerr effect (in plane remanence and coercitivity), both in good agreement with a simple model with one dimensional dependence of the magnetization. Above the critical thickness, MFM observations demonstrate that the stripe width exhibits almost exactly a square root dependence upon thickness. Near to the critical thickness, this allows the stabilisation of very thin magnetic stripes (width down to 38 nm). It is worth noting that the reorientation of the magnetization occurs progressively, but essentially within a limited thickness range (between 29 and 45 nm) and this is in strong discrepancy with a model assuming a one dimensional dependence of the magnetization vector. Since such a model also underestimates the experimentally observed stripe width, this may be seen as a strong indication of the presence of closure domains. Indeed, such closure domains diminish the cost in magnetostatic energy of the magnetic structure, thereby allowing the stabilisation of wider stripes and an higher emergence angle of the magnetization with respect to the layer plane.

Appendix

Here, we demonstrate that the critical thickness does not depend on the sinus-Jacobi form of the magnetization profile (as long as it is a function of the x-coordinate only, the x-axis being within the layer plane). Indeed, the general expression for the energy is the following:

$$E \propto \frac{1}{P}\int_0^P \left[A\left(\frac{\partial\theta(x)}{\partial x}\right)^2 - K_\mathrm{u}\sin^2\theta(x) + E_\mathrm{d}(x)\right]\mathrm{d}x \tag{A.1}$$

with $\theta(x)$ being the local angle of the magnetization vector with respect to the layer plane. P is the period of the magnetization profile.

By taking the magnetization profile: $\sin\ \theta(x) = \sin\ \theta_\mathrm{m}\sin(qx)$, where $q = \pi/d$ (d being the domain width), with the approximation $\sin\ \theta_\mathrm{m} \sim \theta_\mathrm{m}$ which is valid as long as the emergence angle stays low, the dipolar energy can be written:

$$E_\mathrm{d}(x) = [2\pi M_\mathrm{s}^2]\frac{(1-\exp(-hq))(\theta_\mathrm{m}^2\sin^2(qx))}{hq}\,. \tag{A.2}$$

This leads to:

$$E \propto [2\pi M_\mathrm{s}^2]\frac{\theta_\mathrm{m}^2}{2}\left(h^2q^2 - \hat{K}_\mathrm{u} + \frac{1-\exp(-hq)}{hq}\right). \tag{A.3}$$

And, by looking to the instability limit ($E(h,q) = 0$ and $\partial E/\partial h = 0$), one obtains again equations (1, 2).

References

1. A. Cebollada, D. Weller, J. Sticht, G.R. Harp. R.F.C. Farrow, R.F. Marks, R. Savoy, J.C. Scott, Phys. Rev. B **50**, 3419 (1994).
2. B.M. Lairson, B.M. Clemens, Appl. Phys. Lett. **63**, 1438 (1993).
3. S. Mitani, K. Takanashi, M. Sano, H. Fujimori, A. Osawa, H. Nakajima, J. Magn. Magn. Mater. **148**, 163 (1995).
4. K. Takanashi, S. Mitani, M. Sano, H. Fujimori, H. Nakajima, A. Osawa, Appl. Phys. Lett. **67**, 1016 (1995).
5. F.C. Nix, W. Shockley, Rev. Mod. Phys. **10**, 1 (1938).
6. N. Miyata, H. Asami, T. Misushima, K. Sato, J. Phys. Soc. Jpn **59**, 1817 (1990).
7. B. Zhang, W.A. Soffa, Scri. Metall. Mater. **30**, 683 (1994).
8. V. Gehanno, A. Marty, B. Gilles, Y. Samson, Phys. Rev. B **55**, 12 552 (1997).
9. V. Gehanno, Y. Samson, A. Marty, B. Gilles, A. Chamberod, J. Magn. Magn. Mater. **172**, 26 (1997).
10. R.F.C. Farrow, D. Weller, R.F. Marks, M.F. Toney, S. Horn, G.R. Harp, A. Cebollada, Appl. Phys. Lett. **69**, 1166 (1996).
11. V. Gehanno, C. Revenant-Brizard, A. Marty, B. Gilles, J. Appl. Phys. **84**, 2316 (1998).
12. R.P. Cowburn, J. Ferré, J.-P. Jamet, S.J. Gray, J.A.C. Bland, Phys. Rev. B **55**, 11593 (1997).
13. A.L. Sukstanskii, K.I. Primak, J. Magn. Magn. Mater. **169**, 31 (1997).

14. A. Kussmann, K. Jessen, Phys. **17**, 509 (1964).
15. N. Miyata, H. Asami, T. Mizushima, J. Phys. Soc. Jpn **59**, 1817 (1990).
16. B. Zhang, W.A Soffa, Scr. Met. Mater. **128**, 391 (1993).
17. S. Chikazumi, *Physics of Magnetism* (J. Willey & Sons, Inc., 1964).
18. J. Kaczer, M. Zeleny, P. Suda, Czech. J. Phys. B **13**, 579 (1963).
19. M. Hehn, S. Padovani, K. Ounadjela, J.P. Bucher, Phys. Rev. B **54**, 3428 (1996).
20. J.R. Childress, J.L. Duvail, S. Jasmin, A. Barthélémy, A. Fert, A. Schul, O. Durand, P. Galtier, J. Appl. Phys. **75**, 6412 (1994).
21. M. Maret, M.C. Cadeville, R. Poinsot, A. Herr, E. Beaurepaire, C. Monier, J. Magn. Magn. Mater. **166**, 45 (1997).